Polymer Chemistry

PAPER

View Article Online
View Journal | View Issue

Cite this: *Polym. Chem.*, 2016, **7**, 4515

Dramatically different charge transport properties of bisthienyl diketopyrrolopyrrole-bithiazole copolymers synthesized *via* two direct (hetero)-arylation polymerization routes†

Chang Guo, Jesse Quinn, Bin Sun and Yuning Li*

Received 29th April 2016,
Accepted 10th June 2016

DOI: 10.1039/c6py00762g

www.rsc.org/polymers

Two bisthienyl diketopyrrolopyrrole (DPP)-bithiazole based copolymers were synthesised *via* two different direct (hetero)arylation polymerization (DHAP) routes. When a bisthienyl DPP and 5,5′-dibromo-2,2′-bithiazole were used as monomers, the resulting polymer **PA-1** showed poor solubility, ill-organized chain ordering and low performance in organic thin film transistors (OTFTs). Surprisingly, the synthetic route using a dibrominated bisthienyl DPP and 2,2′-bithiazole as monomers produced a polymer **PB-1** with improved solubility, much higher crystallinity and excellent charge transport performance in OTFTs. The electron and hole mobilities of up to 0.53 $cm^2\ V^{-1}\ s^{-1}$ and 0.06 $cm^2\ V^{-1}\ s^{-1}$, respectively, achieved for **PB-1** are more than one order of magnitude higher than those of **PA-1** and also better than the mobilities reported for a similar polymer synthesized *via* Stille coupling polymerization. The dramatically different carrier mobilities observed for these two polymers are accounted for by their different amounts of α–β coupling linkages and branched (and lightly cross-linked) structure defects formed in the respective synthetic routes. This work also demonstrated for the first time that 2,2′-bithiazole is a suitable monomer for the construction of conjugated polymers with good electron transport performance *via* DHAP.

Introduction

Polymer semiconductors have been widely studied as active materials for solution processable organic electronics such as organic thin film transistors (OTFTs),[1–5] organic photovoltaics (OPVs)[6–9] and chemical sensors.[10–13] Compared to small molecules, polymers have better mechanical, thermal and thin-film forming properties, allowing for the fabrication of low-cost, large-area and flexible electronics using various printing technologies such as screen, inkjet or gravure printing.[14,15] To enhance charge carrier mobility, electron-donating and electron-accepting building blocks can be combined in the repeat units to form donor–acceptor (D–A) polymers to shorten the π-stacking distance for more efficient charge hopping.[1,16,17] Diketopyrrolopyrrole (DPP) has been widely used as an electron-acceptor building block for the development of high-performance polymeric semiconductors for OTFTs and OPVs.[4,17–23] The majority of the DPP-based polymers reported in the literature were synthesized using either Suzuki or Stille coupling polymerization, which requires tedious steps to synthesize the organoboron or organotin monomers. Many organotin compounds are known to be highly toxic and are environmental hazards. Recently, a new alternative method, direct (hetero)arylation polymerization (DHAP),[24–27] has been explored to construct conjugated polymers useful for organic electronics.[28–33] Since DHAP involves the C–C bond formation through a coupling reaction between a C–H bond in one conjugated monomer (an arene or heteroarene) and a C–X bond (X is usually a halide, Br or I) in another, this new method is much more environmentally friendly and cost effective than the Suzuki and Stille coupling methods.

Compared to thiophene, which is a commonly used electron donor building block, thiazole is a weak acceptor[34] and has been utilized to promote the electron transport performance of polymer semiconductors.[30,35,36] Previously, DPP-quaterthiophene based conjugating polymers (**PDQT**)[19,37,38] were reported to show p-type hole transport performance with high mobility up to 6.9 $cm^2\ V^{-1}\ s^{-1}$.[37] If a bithiophene unit in **PDQT** is replaced by a 2,2′-bithiazole or 5,5′-bithiazole unit (Fig. 1), the resulting polymer **PDBTz** or **PDBTz′** is expected to show electron transport behaviour. Very recently, a **PDBTz** polymer, **PDBTz-27** (R = 5-decylheptadecyl) synthesized *via* Stille coupling polymerization was reported by Reichmanis

Department of Chemical Engineering and Waterloo Institute for nanotechnology (WIN), University of Waterloo, 200 University Ave West ON, Waterloo, Canada, N2L 3G1. E-mail: yuning.li@uwaterloo.ca; Fax: +1-519-888-4347; Tel: +1-519-888-4567 ext. 31105

†Electronic supplementary information (ESI) available: NMR, AFM, TGA and DSC. See DOI: 10.1039/c6py00762g

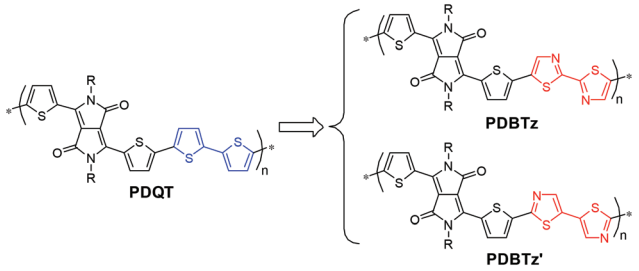

Fig. 1 Structures of DPP-quaterthiophene based polymer **PDQT** and bisthienyl DPP-bithiazole based polymers **PDBTz** and **PDBTz'**, whereas R is an alkyl chain.

and coworkers,[39] which showed high electron mobility of up to 0.3 $cm^2 V^{-1} s^{-1}$ in OTFT devices. In this study, we used the DHAP method through two different routes to prepare two **PDBTz** polymers, **PA-1** and **PB-1** (R = 2-decyltetradecyl). The syntheses of these polymers reported here involved fewer steps than the Stille coupling method. It was found that **PB-1** showed much higher electron mobility of up to 0.53 $cm^2 V^{-1} s^{-1}$ in OTFT devices due to its less structural defects formed during the polymerization compared to **PA-1**.

Results and discussion

The synthetic routes to polymers **PA-1** and **PB-1** are outlined in Scheme 1. Stannylation of 2-bromothiazole resulted in compound **1**, which was coupled with 2-bromothiazole to afford compound **2** in 78% yield. Compound **2** was then brominated

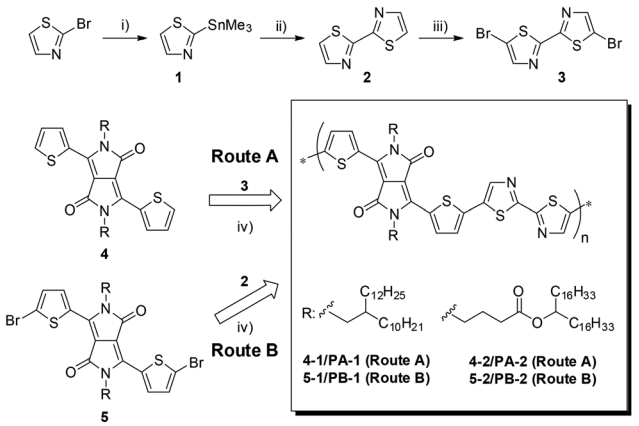

	Yield, %			M_n/PDI	
	CF	TCE	Insol.	CF	TCE
PA-1	9	53	~38	17k/6.9	11k/5.9
PB-1	66	10	~24	18k/3.8	23k/3.9

	Yield, %		M_n/PDI
	HEX	Insol.	HEX
PA-2	81	~19	15k/4.3
PB-2	89	~11	11k/2.5

Scheme 1 Synthetic routes to **PA-1**, **PB-1**, **PA-2** and **PB-2**: (i) *n*-butyllithium/trimethyltin chloride/ether/−78 °C; (ii) $Pd(PPh_3)_4$/toluene/reflux; (iii) NBS/DMF/60 °C; (iv) Herrmann–Beller's catalyst/tris(*o*-methoxyphenyl)phosphine/cesium carbonate/pivalic acid/toluene/reflux. Inserted table shows the yields of the polymer fractions extracted with chloroform (CF) and 1,1,2,2-tetrachloroethane (TCE) as well as the insoluble fractions.

at the 5,5′-positions using *N*-bromosuccinimide (NBS) to form compound **3** in 98% yield. The bithiazole compounds **2** and **3** are monomers for the following DHAP polymerization reactions. The DPP-containing monomers, compounds **4-1** and **5-1**, were prepared according to the literature methods.[37] The target polymers **PA-1** and **PB-1** could be synthesized *via* DHAP through two routes: (A) coupling between **3** and **4-1** to afford **PA-1** and (B) coupling between **2** and **5-1** to afford **PB-1**.

The α C–H bond (at the C2 or C5 position) of thiophene is known to have higher activity toward a C–X (Br or I) bond through DHAP than the β C–H bond (at the C3 or C4 position), allowing for synthesis of soluble polymers with minimal cross-linked structural defects under certain controlled conditions.[31,33,40–43] Monomer **4-1** in Route A has two α C–H bonds and four β C–H bonds in two thiophene units. If DHAP occurs predominantly at the desired α C–H bonds, a linear polymer **PA-1** could be obtained. The regioselectivity of the α C–H bond (at C2 or C5) over the β C–H bond (at C4) in thiazole has also been reported to be very high in DHA reactions for small molecule syntheses.[44–53] A bithiazole compound with the C4 positions substituted (blocked) with nonyl side chains was used for DHAP to make a soluble conjugated polymer without observable cross-linking side reactions.[54] However, to the best of our knowledge, the use of a thiazole compound containing both α and β C–H bonds as a monomer for DHAP has not been demonstrated yet. Therefore, it is interesting to explore if the use of a β non-substituted bithiazole compound **2** as a monomer in Route B can form a soluble target polymer **PB-1**.

Two polymerization reactions were conducted under identical conditions, in the presence of a catalyst system containing *trans*-bis(acetato)bis[*o*-(di-*o*-tolylphosphino)benzyl]dipalladium (II) (Herrmann–Beller's catalyst), tris(*o*-methoxyphenyl)phosphine, cesium carbonate and pivalic acid under reflux in toluene for 16 h, which were successfully used for the preparation of other conjugated polymers through DHAP.[29–32,55] The crude polymers were purified by Soxhlet extraction using acetone, hexane, chloroform and 1,1,2,2-tetrachloroethane (TCE) sequentially. Negligible amounts of polymers were dissolved by acetone and hexane. For **PA-1**, 9% was dissolved by chloroform and 53% by TCE. The remaining (~38%) solid was insoluble in common known solvents. **PB-1** showed much improved solubility with 66% dissolved in chloroform and 10% dissolved in TCE, but ~24% of this polymer still remained insoluble (Scheme 1). High temperature gel permeation chromatography (HT-GPC) with 1,2,4-trichlorobenzene as an eluent and polystyrene as standards at a column temperature of 140 °C was used to determine the molecular weights of **PA-1** and **PB-1** due to the strong chain aggregation tendency at room temperature. The number-average molecular weight (M_n)/polydispersity index (PDI) of **PA-1** are 17 kDa/6.9 for the chloroform extracted fraction and 11 kDa/5.9 for the TCE extracted fraction. M_n/PDI of **PB-1** are 18 kDa/3.8 for the chloroform extracted fraction and 23 kDa/3.9 for the TCE extracted fraction (Scheme 1).

As aforementioned, one immensely important issue associated with DHAP is that side reactions of C–X (X = Br or I) bonds with the undesirable (hetero)aromatic C–H bonds, such

as the β C–H at the C3 or C4 position in thiophene,[56] can occur, leading to formation of cross-linked, insoluble polymers and low molecular weight soluble fractions.[32,40,54,57–59] Therefore, a possible reason for the presence of a significant amount of insoluble fractions for both polymers (**PA-1**: ~38%; **PB-1**: ~24%) is due to the formation of cross-linked structures *via* the side reactions between the α C–Br and the β C–H bonds on thiophene and/or thiazole units. **PB-1** showed much better solubility and narrower molecular weight distributions for its soluble fractions in chloroform and TCE compared with **PA-1**, indicating that less α–β coupling side reactions might have occurred in Route B.

^{1}H-NMR spectroscopy has been used to determine the presence of branched structures formed *via* α–β coupling side reactions of thiophene units.[38,40,60,61] However, the ^{1}H NMR spectra of these two polymers acquired at room temperature showed extremely poor resolutions due to the aggregation of polymer chains, which has been reported for some other D–A polymers.[19,62] To improve the spectral resolution, the NMR measurements were conducted at an elevated temperature of 120 °C. Three major peaks at 7.43, 8.09 and 8.82 ppm are clearly seen for both polymers, which can be assigned to H_a and H_c in the thiophene units and H_b in the thiazole units (Fig. 2). However, several minor peaks, which appear at different positions for **PA-1** and **PB-1**, are also observed. These may be originated from their different terminal monomer units and α–β coupled units. However, it is very difficult to assign the peaks that belong to the α–β coupling structures.

Another possible reason for the large amounts of insoluble products in **PA-1** and **PB-1** is due to the poor solubility of their high molecular weight fractions. To confirm if the formation of insoluble fractions was caused by cross-linking or the high molecular weights, two model polymers **PA-2** and **PB-2** with much larger tritriacontan-17-yl butyrate side chains[63] were synthesized under the same reaction conditions used for **PA-1** and **PB-1** (Scheme 1). Most of **PA-2** (81%) and **PB-2** (89%) could be dissolved with hexane by Soxhlet extraction, indicating the greatly improved solubility of these two polymers. However, there were still some remaining products, which could not be dissolved by any solvent, for both polymers (**PA-2**: ~19%; **PB-2**: ~11%). Since the solubility of these soluble fractions is excellent (soluble in hexane at room temperature) due to their large side chains, the presence of insoluble products is considered to be caused by the cross-linking of the polymer chains by the side reactions rather than by their high molecular weights. The soluble fractions of these two polymers were subject to the GPC measurements. M_n/PDI values of 15 kDa/4.3 for **PA-2** and 11 kDa/2.5 for **PB-2** were obtained, which are comparable to the values for **PA-1** and **PB-1**, even though the solubility of these two model polymers is much improved. This could be explained by the premature termination of the polymer chain growth during the polymerization. Since both polymers contain appreciable amounts of insoluble fractions, it is reasonable to consider that cross-linking occurred during the polymerization, which resulted in the formation of some insoluble polymer chains containing heavily cross-linked struc-

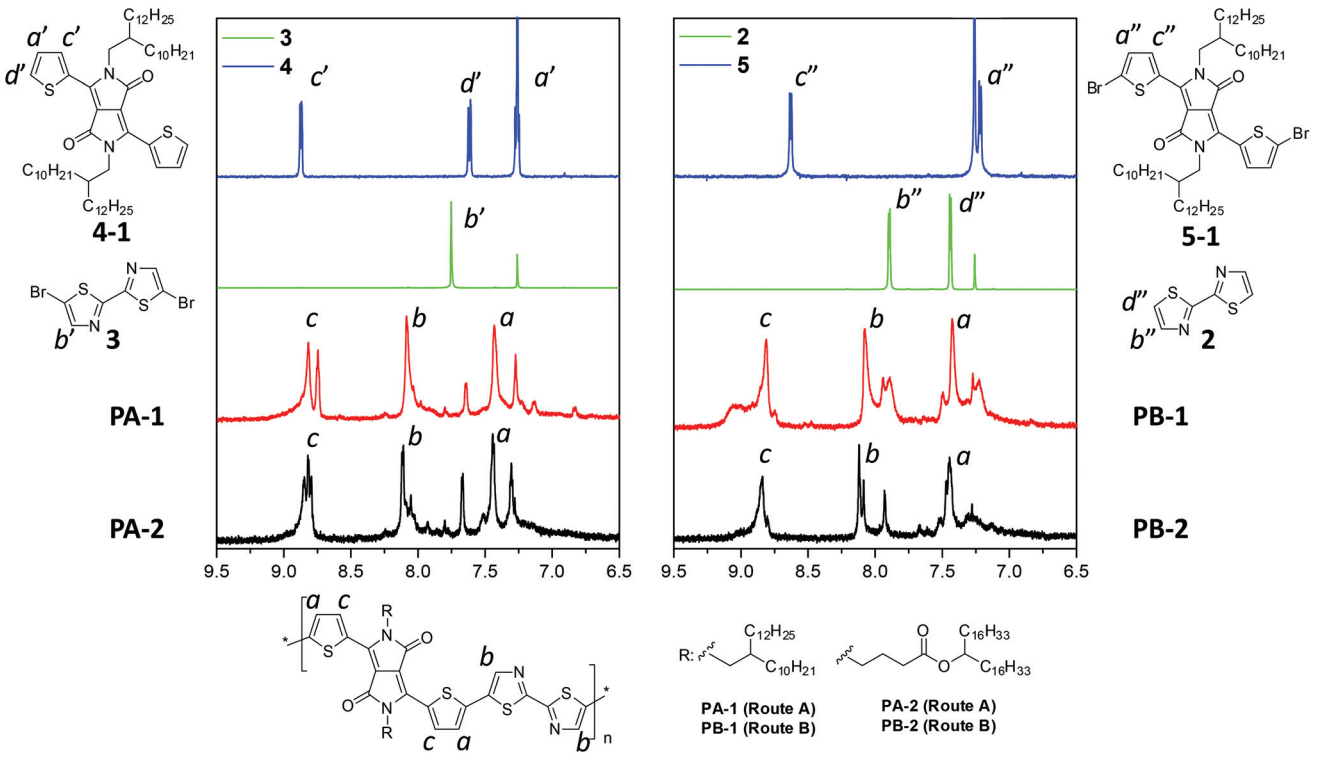

Fig. 2 The ^{1}H-NMR spectra of polymers **PA-1**, **PB-1**, **PA-2**, **PB-2**, and monomers **2**, **3**, **4-1** and **5-1**. The measurements were carried out at 120 °C for the polymers and at room temperature for the monomers.

tures. Due to the excessive consumption of the C–Br groups by the cross-linked structures through α–β coupling, the remaining polymer chains did not have functional C–Br groups for further growth and consequently led to their smaller molecular weights. Because the solubility of **PA-2** and **PB-2** is much improved, their ^{1}H-NMR spectra were measured in order to elucidate the defective structures formed by the side reactions. However, the ^{1}H-NMR spectra of **PA-2** and **PB-2** are very similar to those of their corresponding polymers, **PA-1** and **PB-1** (Fig. 2), although the peaks of **PA-2** and **PB-2** are sharper as a result of their improved solubility. The major peaks, a, b, and c, are assigned as shown in Fig. 2 according to the NMR spectra of their corresponding monomers. The minor peaks at 7.3 ppm and 7.7 ppm for **PA-1** and **PA-2** are positioned similarly to those of the peaks of a′ and d′ of **4-1** and **4-2** (not shown), suggesting that **4-1** (or **4-2**) is a terminal unit in **PA-1** (or **PA-2**). On the other hand, there is only a very small peak at ~7.8 ppm that is close to the chemical shift of peak b′ of **3**, indicating that the amount of **3** as a terminal unit in **PA-1** and **PA-2** is minimal. For **PB-1** and **PB-2**, the peak at 7.9 ppm could be assigned to the β-H b″ of the terminal **2** unit, while the α-H of the terminal **2** unit might be hidden in peak a. On the contrary, there is no peak that corresponds to c″ of monomer **5-1**, suggesting that **5-1** is unlikely a terminal unit in **PB-1** and **PB-2**. The above observations indicate that **4-1** and **4-2** are the dominant terminal units for **PA-1** and **PA-2**, respectively, while **2** is the dominant terminal unit for **PB-1** and **PB-2**. The lack of the dibromo monomer terminal units (**3**, **5-1** or **5-2**) substantiates that some of the C–Br bonds reacted with β-H′s. The α-H in an α–β coupling defect could further react with a C–Br group, consequently forming branched and crosslinked structures (see Scheme S1 in the ESI†). It should be noted that the major peaks, a, b, and c, are comprised of multiple peaks and/or minor peaks, which might be originated from the sub-terminal units and the branched (or lightly cross-linked) structures formed by α–β coupling. Therefore, we may conclude that both polymerization routes (A and B) likely involved the α–β coupling reactions that led to the formation of cross-linked structures, whereas the polymers produced in Route A have more cross-linked structures than the polymers made by Route B based on the amounts of their insoluble fractions. Polymer chains in the soluble fractions may also contain structural defects such as branches and lightly cross-linked structures.

The branched and lightly cross-linked structures would cause twisting of the polymer backbone, while the α–β coupling linkages in the polymer backbone would disrupt the π-conjugation. As a result, the optical band gap of the polymer with more structural defects would be larger. To confirm this, UV-Vis absorption spectra of these polymers were measured in their dilute chloroform solutions and thin films. The wavelength of maximum absorbance (λ_{max}) of **PA-1** was observed at 660 nm in solution and 746 nm in the thin film (Fig. 3a). **PB-1** showed a longer λ_{max} at 677 nm in solution. The as-cast film of **PB-1** exhibited a λ_{max} at 737 nm, which is shorter than that of the **PA-1** film. However, the right side of the absorption spectrum of the **PB-1** film extends farther into the near infrared

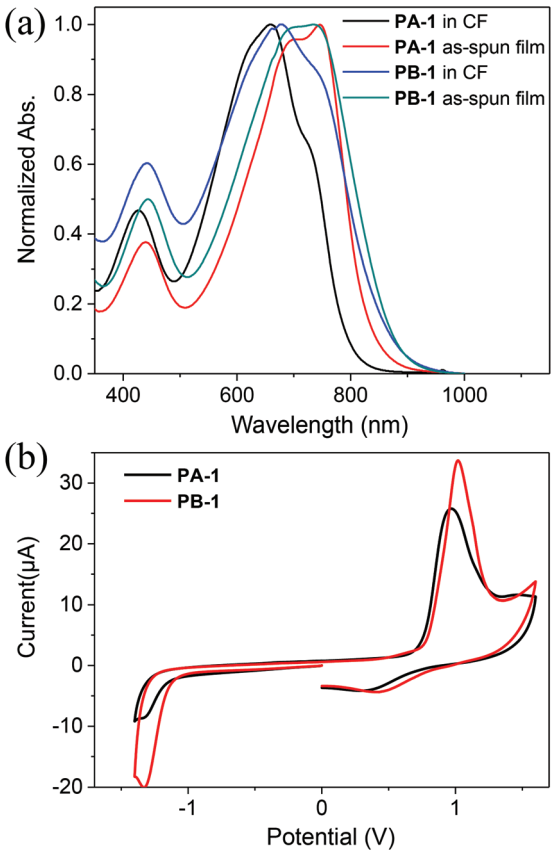

Fig. 3 (a) UV-Vis absorption spectra of **PA-1** and **PB-1** in chloroform solutions and in thin films; (b) cyclic voltammograms of as-cast **PA-1** and **PB-1** films measured in anhydrous CH_3CN solution using Bu_4NPF_6 as the electrolyte.

region than the **PA-1** film. As a result, the optical band gap of **PB-1** (1.42 eV) is narrower than that of **PA-1** (1.49 eV) calculated using the onset absorption wavelengths of their films. The larger optical band gap of **PA-1** suggests its shorter effective conjugation length than that of **PB-1**. Because the M_n's of **PA-1** and **PB-1** extracted with chloroform are very similar (17 kDa *vs.* 18 kDa) and the weight-average molecular weight (M_w) of **PA-1** (117 kDa) is much larger than that of **PB-1** (70 kDa), the effective conjugation length of **PA-1** should be similar or larger than that of **PB-1** if both polymers have linear main chain structures. Therefore, the blue-shift of the absorption spectrum of **PA-1** seems to support the assumption that **PA-1** contains more α–β coupling defects in the main chain and/or branched (and lightly cross-linked) structures, which disrupted the main chain conjugation. Due to the influence of the large side chains, the λ_{max}'s of **PA-2** in solution (617 nm) and in the film (665 nm) (Fig. S8†) are both shorter than those of **PA-1**. The same trend is observed for **PB-2**, which showed shorter λ_{max}'s of 650 nm in solution and 685 nm in the film compared to **PB-1**. However, it is obvious that the spectra of **PA-2** showed significant blue shifts in both solution and film with respect to those of **PB-2**, similar to the trend observed for **PA-1** and **PB-1**. The optical band gap of **PA-2** (1.54 eV) is thus wider than

that of **PB-2** (1.50 eV), indicating again the presence of more α–β coupling defects and/or branched (and lightly cross-linked) structures in **PA-2** obtained by Route B.

Cyclic voltammetry (CV) was used to determine the frontier energy levels of **PA-1** and **PB-1** films (Fig. 3b). By using the onset oxidative/reductive potentials, the HOMO/LUMO levels are calculated to be −5.55 eV/−3.61 eV for **PA-1** and −5.56 eV/−3.63 eV for **PB-1**, respectively. The energy levels of **PA-1** and **PB-1** are very similar and also close to those of the DPP-bithiazole copolymer **PDBTz-27** (R = 5-decylheptadecyl) obtained by Stille coupling (E_{HOMO}/E_{LUMO} = −5.54 eV/−3.75 eV).[39] The HOMO levels of **PA-1** and **PB-1** are lower compared to their thiophene analogue **PDQT-24** (−5.33 eV)[37] due to the presence of the electron-deficient bithiazole units.[34]

The atomic force microscopy (AFM) images (Fig. S9†) of **PA-1** and **PB-1** showed that all the polymer thin films are very smooth and did not undergo dramatic morphological changes after annealed at temperatures ranging from 100 °C to 250 °C. The crystallinity of the polymer thin films was investigated by reflection X-ray diffractometry (XRD). The **PA-1** film annealed at 100 °C showed no obvious diffraction peaks, indicating its very poor crystallinity (Fig. 4a). When the annealing temperature was increased to 150 °C, a weak primary (100) peak appeared at 2θ = 3.85°, which corresponds to a *d*-spacing distance of 2.29 nm. By increasing the annealing temperature to 200 °C, the crystallinity of the **PA-1** film improved notably, as evidenced by the much intensified peak at 2θ = 3.94° (*d*-spacing = 2.24 nm). Further increasing the annealing temperature to 250 °C, the intensity of the primary peak and the *d*-spacing remained almost the same. As shown in Fig. 4b, the reflection XRD pattern of the **PB-1** thin film annealed at 100 °C exhibited a small peak at 2θ = 3.69°, which corresponds to a *d*-spacing of 2.39 nm. As the annealing temperature increased to 150 °C, the primary peak intensified significantly and the peak shifted slightly to 2θ = 3.93°, which corresponds to a much shorter *d*-spacing distance of 2.25 nm. Upon annealing at higher temperatures of 200 and 250 °C, a continued increase in the intensity of the primary peak as well as a shift of this peak to 2θ = 3.99° (*d*-spacing = 2.21 nm) and 4.05° (*d*-spacing = 2.18 nm) were observed. A noticeable secondary peak also appeared. This manifests that the polymer chains were packed much more orderly and compactly with the aid of thermal annealing at high temperatures. The significantly higher crystallinity of the **PB-1** films than that of the **PA-1** films annealed at the same temperatures most likely resulted from the presence of less α–β coupling linkages and branched (and lightly-cross-linked) structural defects in the former as discussed previously. Since no (010) peaks can be seen, the polymer chains of **PA-1** and **PB-1** in the spin-coated thin film samples presumably adopted a layer-by-layer lamellar packing motif with an edge-on orientation, which has been observed for other crystalline conjugated polymers.[64,65] To elucidate the in-plane chain packing motif, we measured the 250 °C-annealed **PA-1** and **PB-1** flakes using transmission XRD (Fig. 4c). Both polymers showed a broad peak around 2θ = ~20° (*d*-spacing = 0.44 nm), which represents the typical van der Waals distance for an amorphous polymer phase. The 250 °C-annealed **PB-1** flakes showed a distinct (010) peak at 24.6°, which corresponds to a π–π stacking distance of 0.36 nm. **PA-1**, on the other hand, exhibited a small hump at the similar position, suggesting that the polymer main chains are much less orderly packed along the π–π stacking direction in this polymer. Again, the presence of more α–β coupling linkages and branched (and lightly cross-linked) structural defects in **PA-1** would sterically hinder the π–π stacking of the polymer main chains. It is noticed that the π–π stacking distance of these polymers is smaller than that of **PDQT-24** (0.39 nm),[37] indicating the stronger intermolecular interaction in the **PDBTz** polymers.

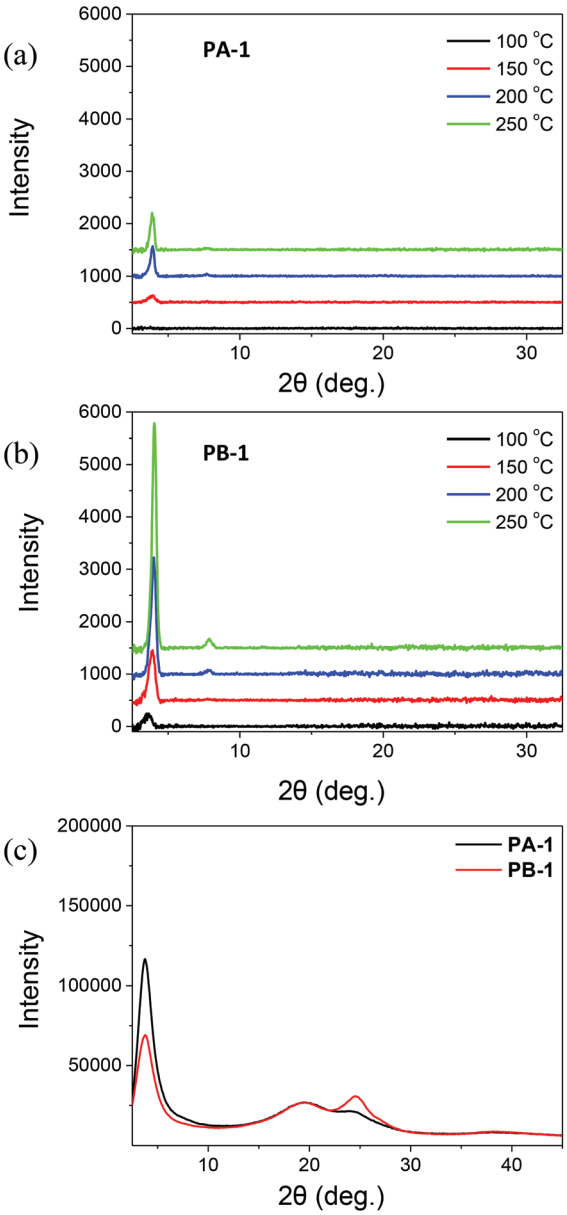

Fig. 4 **PA-1** (a) and **PB-1** (b) thin films (~40 nm) on SiO_2/Si substrates, and transmission (in-plane) diagrams (c) of 250 °C-annealed **PA-1** and **PB-1** flakes.

Table 1 Performance of OTFT devices using **PA-1** and **PB-1** annealed at different temperatures

Polymer	Annealing temperature (°C)	Average electron mobility (standard deviation) ($cm^2 V^{-1} s^{-1}$)	Maximum electron mobility ($cm^2 V^{-1} s^{-1}$)	I_{on}/I_{off}	Average hole mobility (standard deviation) ($cm^2 V^{-1} s^{-1}$)	Maximum hole mobility ($cm^2 V^{-1} s^{-1}$)	I_{on}/I_{off}
PA-1	100	3.3×10^{-3} (6.7×10^{-4})	3.7×10^{-3}	~10^5	5.7×10^{-4} (1.3×10^{-4})	7.2×10^{-4}	~10^6
	150	1.3×10^{-2} (5.8×10^{-4})	1.3×10^{-2}	~10^5	3.0×10^{-4} (1.1×10^{-4})	3.0×10^{-4}	~10^6
	200	2.3×10^{-2} (1.1×10^{-2})	3.9×10^{-2}	~10^5	3.8×10^{-4} (1.9×10^{-4})	5.5×10^{-4}	~10^5
	250	2.4×10^{-2} (9.2×10^{-3})	3.9×10^{-2}	~10^6	2.0×10^{-3} (2.6×10^{-4})	2.4×10^{-3}	~10^6
PB-1	100	1.6×10^{-2} (1.2×10^{-3})	1.7×10^{-2}	~10^5	7.0×10^{-3} (1.7×10^{-3})	8.9×10^{-3}	~10^5
	150	7.9×10^{-2} (1.1×10^{-2})	9.2×10^{-2}	~10^6	7.0×10^{-3} (3.5×10^{-3})	1.1×10^{-2}	~10^6
	200	7.9×10^{-2} (2.3×10^{-2})	0.11	~10^6	7.0×10^{-3} (1.1×10^{-3})	8.2×10^{-3}	~10^6
	250	0.42 (0.11)	0.53	~10^5	4.8×10^{-2} (1.1×10^{-2})	5.9×10^{-2}	~10^6

To evaluate the charge transport performance of **PA-1** and **PB-1**, we used these two polymers as channel semiconductors in top-gate, bottom-contact OTFT devices. The Au source and drain electrodes were deposited on a SiO_2/Si wafer substrate by a common photolithography method. A solution of **PA-1** or **PB-1** in chloroform (10 mg mL^{-1}) was spin-coated on the substrate to obtain a polymer thin film (~40 nm), which was annealed at 100 °C, 150 °C, 200 °C or 250 °C for 15 min on a hotplate in nitrogen. Then the gate dielectric layer (~570 nm) was formed by spin-coating a Cytop (a fluoropolymer) solution at 2000 rpm. After baking on a hotplate at 100 °C for 1 h in nitrogen, a ~70 nm Al layer was deposited by thermal evaporation as the gate electrode. The devices were characterized in air in the absence of light. In contrast with **PDQT** that showed unipolar hole transport performance,[19,37,38] all devices of **PA-1** and **PB-1** exhibited ambipolar charge transport behaviour with more pronounced electron transport over hole transport (Table 1), which is a result of the presence of electron-deficient bithiazole units. In the n-channel operation mode, devices based on the **PA-1** thin films showed electron mobility of up to 3.7×10^{-3} $cm^2 V^{-1} s^{-1}$ for the 100 °C-annealed films. The mobility improved as the annealing temperature increased. The highest electron mobility of 2.4×10^{-2} $cm^2 V^{-1} s^{-1}$ was achieved for a 250 °C-annealed film. On the other hand, **PB-1** showed much superior electron transport performance. The average electron mobility increased from 1.6×10^{-2} $cm^2 V^{-1} s^{-1}$ for the 100 °C-annealed films to 0.42 $cm^2 V^{-1} s^{-1}$ for the 250 °C-annealed films. The maximum electron mobility of ~0.53 $cm^2 V^{-1} s^{-1}$ was achieved for a 250 °C-annealed **PB-1** film (Fig. 5). In the p-channel operation mode, both polymers showed hole transport characteristics, but their hole mobilities are about one order of magnitude lower than their respective electron mobilities at the same annealing temperatures. The best hole mobilities are 2.4×10^{-3} $cm^2 V^{-1} s^{-1}$ for **PA-1** and 5.9×10^{-2} $cm^2 V^{-1} s^{-1}$ for **PB-1**, both achieved for the films annealed at 250 °C. The significantly lower charge transport performance shown by **PA-1** is considered primarily due to the presence of a larger amount of irregular α–β coupling linkages and branched (and lightly cross-linked) structures, which reduced the main chain conjugation length and resulted in disordered chain ordering as revealed by the UV-Vis and XRD data. Polymer thin films annealed at a higher temperature of 300 °C were also tested, but the mobility values dropped.

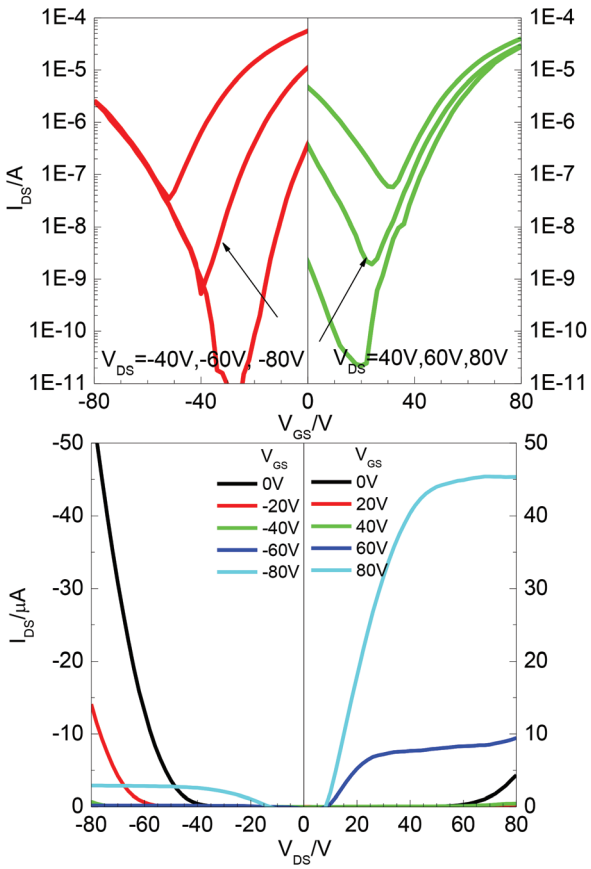

Fig. 5 Transfer (a) and output curves (b) of OTFT devices with **PB-1** thin films annealed at 250 °C for 15 min. Device dimensions: channel width (W) = 1 mm; channel length (L) = 30 μm.

Because both **PA-1** and **PB-1** showed very good thermal stability with a 5% weight loss at 395 °C and 384 °C, respectively (see the thermogravimetric analysis (TGA) thermograms in Fig. S16†), the drop in mobility for the 300 °C-annealed polymer films is presumably due to the deteriorated semiconductor/dielectric or semiconductor/electrode interface. Devices based on the **PA-2** and **PB-2** thin films showed electron mobilities of up to 1.7×10^{-4} and 3.3×10^{-3} $cm^2 V^{-1} s^{-1}$, respectively, for the 250 °C-annealed films. Negligible hole transport performance was observed. The much lower mobili-

ties compared to **PA-1** and **PB-1** are due to the adverse effect of the large side chains on the chain packing. Nonetheless, the charge transport performance of **PA-2** is still significantly lower than that of **PB-2**, since Route A produced more irregular coupling linkages.

Experimental

Materials and characterization

All chemicals were purchased from Sigma Aldrich and other commercial sources and used without further purification. Cytop (a perfluorinated amorphous resin) was purchased from AGC Chemicals. Compounds **4-1** and **5-1** were prepared according to the literature methods.[37] NMR spectra were recorded on a Bruker DPX 300 MHz spectrometer with chemical shifts relative to tetramethylsilane (TMS, 0 ppm). UV-Vis spectra were collected by a Thermo Scientific GENESYS-20 spectrophotometer. Cyclic voltammetry (CV) data were obtained with a CHI600E electrochemical analyser using an Ag/AgCl reference electrode, a Pt wire counter electrode, and a Pt foil working electrode in 0.1 M tetrabutylammonium hexafluorophosphate in anhydrous acetonitrile at a sweep rate of 50 mV s^{-1}. Ferrocene was used as a reference, which has a highest occupied molecular orbital (HOMO) of −4.8 eV.[66] Atomic force microscopy (AFM) images of polymer thin films spin coated on SiO_2/Si substrates were recorded using a Dimension 3100 scanning probe microscope. After the AFM measurements, the reflection X-ray diffraction (XRD) patterns of the polymer samples were characterized using a Bruker D8 Advance powder diffractometer with a standard Bragg–Bretano geometry using Cu Kα radiation (λ = 1.5406 Å). Transmission XRD measurements were conducted on a Bruker Smart 6000 CCD 3-circle D8 diffractometer with a Cu RA (Rigaku) X-ray source (λ = 1.5406 Å) using polymer flakes stacked between two Mylar substrates. Gel-permeation chromatography (GPC) measurements of polymers were performed on a Malvern HT-GPC using 1,2,4-trichlorobenzene as an eluent and polystyrene as standards at 140 °C. The thermogravimetric analysis (TGA) was conducted on a TGA Q500 Thermogravimetric Analyzer (TA Instruments) at a heating rate of 10 °C min^{-1} under nitrogen.

OTFTs fabrication and characterization

A top-gate, bottom-contact OTFT structure with heavily n-doped Si/SiO_2 wafer as the substrate was used to evaluate the charge transport performance of **PA-1** and **PB-1**. The source/drain electrode pairs were deposited using the conventional photolithography method to define the device dimensions with a channel length (L) of 30 μm and a channel width (W) of 1 mm. The substrate was cleaned using acetone and then isopropanol in an ultrasonic bath prior to use. A polymer film with a thickness of ~40 nm was deposited on the substrate by spin coating a polymer solution in chloroform (10 mg mL^{-1}) at 2000 rpm for 60 s and subsequently annealed at 100 °C, 150 °C, 200 °C or 250 °C for 15 min in a glove box. A Cytop layer (~570 nm) as the gate dielectric was then deposited by spin coating a Cytop solution, followed by drying at 100 °C on a hotplate for 1 h in a glove box before thermally depositing an Al gate electrode layer (~70 nm). All devices were characterized in air in the absence of light using an Agilent 4155C Semiconductor Analyser. Carrier mobility was calculated in the saturation regime according to the equation:

$$I_D = \left(\frac{WC_i}{2L}\right)\mu(V_G - V_T)^2$$

where I_D is the drain current, μ is the charge carrier mobility, C_i is the capacitance per unit area of the insulator determined from a metal–insulator–metal structure (C_i is 3.2 nF cm^{-2} for a 570 nm-thick Cytop film) and V_G is the gate voltage.

Synthesis

2-(Trimethylstannyl)thiazole (1). A solution of 2-bromothiazole (1.64 g, 10 mmol) in anhydrous diethyl ether (25 mL) was slowly added into a stirred solution of *n*-butyllithium (4.4 mL, 2.5 M in hexane) in anhydrous diethyl ether (40 mL) at −78 °C. The mixture was stirred for 1 h, then a solution of trimethyltin chloride (11 mL, 1.0 M in hexane) was added dropwise over 15 min. After stirring for an additional hour at −78 °C, the reaction mixture was quenched with saturated aqueous sodium hydrogen carbonate solution (15 mL) and extracted with diethyl ether. The organic layer was dried over anhydrous sodium sulfate and the solvent was removed under reduced pressure. The obtained yellow liquid was directly used in the next step without further purification. Yield: 2.51 g (~100%). ^{1}H NMR (300 MHz, $CDCl_3$) δ 8.15 (d, J = 2.5 Hz, 1H), 7.56 (d, J = 2.7 Hz, 1H), 0.47 (s, 9H). Synthesis of compound **1** was reported previously using a different procedure.[67]

2,2′-Bithiazole (2). A solution of **1** (0.694 g, 2.8 mmol), 2-bromothiazole (0.328 g, 2 mmol) and tetrakis(triphenylphosphine)palladium(0) ($Pd(PPh_3)_4$) (46 mg, 0.05 mmol) in toluene was refluxed for 24 h under a nitrogen atmosphere. The reaction mixture was allowed to cool down to room temperature before the solvent was removed under reduced pressure. The crude product was purified by column chromatography on silica gel with a mixture of hexane and ethyl acetate (v/v = 7/3) as an eluent to give compound **2** as white crystals. Yield: 0.263 g (78.1%). ^{1}H NMR (300 MHz, $CDCl_3$) δ 7.90 (d, J = 3.1 Hz, 2H), 7.44 (d, J = 3.2 Hz, 2H). Synthesis of compound **2** was reported previously using a different procedure.[67]

5,5′-Dibromo-2,2′-bithiazole (3).[67] *N*-Bromosuccinimide (NBS) (0.872 g, 4.9 mmol) was added in portions to a solution of **2** (0.206 g, 1.2 mmol) in *N*,*N*-dimethylformamide (DMF) (10 mL) at room temperature. The reaction mixture was then heated to 60 °C and stirred at this temperature for 5 h. The mixture was poured into water (200 mL) and extracted with dichloromethane. The organic phase was dried over anhydrous sodium sulphate. The crude product was purified by column chromatography on silica gel with a mixture of hexane and ethyl acetate (v/v = 3/1) as an eluent to give compound **3** as yellow crystals. Yield: 0.390 g (98.0%). ^{1}H NMR (300 MHz, $CDCl_3$) δ 7.75 (s, 2H).

Di(tritriacontan-17-yl) 4,4′-(1,4-dioxo-3,6-di(thiophen-2-yl) pyrrolo[3,4-*c*]pyrrole-2,5(1*H*,4*H*)-diyl)dibutanoate (4-2). **4-2** was synthesized following the similar procedure for the synthesis of **4-1** according to the literature methods.[37] Yield: 0.67 g (61.0%). ^{1}H NMR (300 MHz, $CDCl_3$) δ 8.90 (d, J = 3.9 Hz, 2H), 7.64 (d, J = 5.0 Hz, 2H), 7.29 (t, J = 4.6 Hz, 2H), 4.86 (t, J = 6.2 Hz, 2H), 4.15 (t, J = 7.4 Hz, 4H), 2.44 (t, J = 7.6 Hz, 4H), 2.10 (q, J = 7.5 Hz, 4H), 0.87 (t, J = 6.5 Hz, 12H). ^{13}C NMR (75 MHz, $CDCl_3$) δ 172.57, 135.36, 131.01, 128.85, 74.87, 41.62, 34.21, 32.14, 32.09, 29.86, 29.82, 29.77, 29.72, 29.70, 29.52, 25.53, 25.48, 22.85, 14.28. HRMS $(M + H)^+$ Calc. for $C_{88}H_{153}O_6N_2S_2^+$: 1398.1109; found: 1398.1164.

Di(tritriacontan-17-yl) 4,4′-(3,6-bis(5-bromothiophen-2-yl)-1,4-dioxopyrrolo[3,4-*c*]pyrrole-2,5(1*H*,4*H*)-diyl)dibutanoate (5-2). **5-2** was synthesized following the similar procedure for the synthesis of **5-1** according to the literature methods.[37] Yield: 0.41 g (93.0%). ^{1}H NMR (300 MHz, $CDCl_3$) δ 8.63 (d, J = 4.2 Hz, 2H), 7.24 (d, J = 4.3 Hz, 2H), 4.87 (t, J = 6.1 Hz, 2H), 4.07 (t, J = 7.4 Hz, 4H), 2.43 (t, J = 7.4 Hz, 4H), 2.14–1.99 (m, 4H), 0.88 (t, J = 6.6 Hz, 12H). ^{13}C NMR (75 MHz, $CDCl_3$) δ 135.35, 131.92, 131.11, 77.36, 75.00, 41.68, 34.21, 32.09, 32.00, 29.87, 29.83, 29.78, 29.71, 29.53, 25.50, 22.86, 14.28. HRMS $(M + H)^+$ Calc. for $C_{88}H_{151}Br_2O_6N_2S_2^+$: 1553.9302; found: 1553.9345.

Synthesis of PA-1

To a 25 mL Schlenk flask were added compound **3** (24.5 mg, 0.075 mmol), **4-1** (73.0 mg, 0.075 mmol), *trans*-bis(acetato)bis-[*o*-(di-*o*-tolylphosphino)benzyl]dipalladium(II) (Herrmann–Beller's catalyst) (1.4 mg, 1.5 μmol), tris(2-methoxyphenyl) phosphine (2.1 mg, 6.0 μmol), cesium carbonate (56.2 mg, 0.29 mmol), and pivalic acid (2.3 mg, 0.023 mmol). After degassing and refilling argon for 3 times, anhydrous toluene (3 mL) was added under argon. The mixture was refluxed for 16 h. After cooling down to room temperature, the reaction mixture was poured into methanol (100 ml). The precipitates were collected by filtration and subjected to Soxhlet extraction with acetone, hexane, chloroform and TCE. Yield: 7.7 mg (9.0%) from the chloroform-extracted fraction and 45.4 mg (53.2%) from the TCE-extracted fraction. The remaining solid (~38%) is insoluble in any solvent. HT-GPC data: M_n = 17 kDa and PDI = 6.9 (chloroform extracted fraction); M_n = 11 kDa and PDI = 5.9 (TCE extracted fraction).

Synthesis of PA-2

PA-2 was synthesized using compound **3** (24.5 mg, 0.075 mmol) and **4-2** (84.9 mg, 0.075 mmol), following the similar procedure for the synthesis of **PA-1**. Yield: 95.3 mg (81.3%) from the hexane-extracted fraction. The remaining solid (~19%) is insoluble in any solvent. HT-GPC data: M_n = 15 kDa and PDI = 4.3.

Synthesis of PB-1

PB-1 was synthesized using compound **2** (12.6 mg, 0.075 mmol) and **5-1** (84.9 mg, 0.075 mmol), following the similar procedure for the synthesis of **PA-1**. Yield: 56.5 mg (66.2%) from the chloroform-extracted fraction and 8.2 mg (9.6%) from the TCE-extracted fraction. The remaining solid (~24%) is insoluble in any solvent. HT-GPC data: M_n = 18 kDa and PDI = 3.8 (chloroform extracted fraction); M_n = 23 kDa and PDI = 3.9 (TCE extracted fraction).

Synthesis of PB-2

PB-2 was synthesized using compound **2** (12.6 mg, 0.075 mmol) and **5-2** (116.7 mg, 0.075 mmol), following the similar procedure for the synthesis of **PA-1**. Yield: 104.4 mg (89.1%) from the hexane-extracted fraction. The remaining solid (~11%) is insoluble in any solvent. HT-GPC data: M_n = 11 kDa and PDI = 2.5.

Conclusions

We synthesized two bisthienyl DPP-bithiazole copolymers **PA-1** and **PB-1** using the DHAP method *via* two routes. **PA-1** was synthesized by reacting 5,5′-dibromo-2,2′-bithiazole and the DPP monomer, while **PB-1** was synthesized by reacting the dibrominated bisthienyl DPP and 2,2′-bithiazole monomers. It was found that **PA-1** showed a larger band gap, much poorer solubility and lower degree of crystallinity compared to **PB-1**, which were considered to be due to the presence of a larger amount of α–β coupling linkages and branched (and lightly cross-linked) structures in the former. **PB-1**, which has less structural defects, achieved very high ambipolar charge transport performance with electron and hole mobilities of up to 0.53 $cm^2\ V^{-1}\ s^{-1}$ and $5.9 \times 10^{-2}\ cm^2\ V^{-1}\ s^{-1}$, respectively, in OTFT devices. In contrast, **PA-1** showed one order of magnitude lower mobilities. Our results demonstrated that placing the bromo groups on different monomers could significantly influence the occurrence of α–β coupling side reactions, which led to the formation of polymers with dramatically different properties. This work for the first time demonstrated that 2,2′-bithiazole is a suitable monomer with good regioselectivity for the construction of regular conjugated polymers with promoted electron transport performance *via* DHAP. The synthesis of **PDBTz′** (Fig. 1), an isomer of **PDBTz**, by DHAP between 5,5′-bithiazole (or 2,2′-dibromo-5,5′-bithiazole) and the bisthienyl DPP monomer **4-1** (or **5-1**) is under way. Changing the positions of the nitrogen atoms in the bithiazole units may have an impact on the side reactions and the charge transport performance of the resulting polymers.

Acknowledgements

The authors thank the NSERC Discovery Grants (#402566-2011) from the federal government of Canada for the financial support of this research.

Notes and references

1 C. B. Nielsen, M. Turbiez and I. McCulloch, *Adv. Mater.*, 2012, **25**, 1859–1880.

2 C. Guo, W. Hong, H. Aziz and Y. Li, *Rev. Adv. Sci. Eng.*, 2012, **1**, 200–224.
3 J. D. Yuen and F. Wudl, *Energy Environ. Sci.*, 2013, **6**, 392–406.
4 Y. Li, P. Sonar, L. Murphy and W. Hong, *Energy Environ. Sci.*, 2013, **6**, 1684–1710.
5 H. Sirringhaus, *Adv. Mater.*, 2014, **26**, 1319–1335.
6 E. Bundgaard and F. C. Krebs, *Sol. Energy Mater. Sol. Cells*, 2007, **91**, 954–985.
7 R. Kroon, M. Lenes, J. C. Hummelen, P. W. M. Blom and B. de Boer, *Polym. Rev.*, 2008, **48**, 531–582.
8 Y. J. Cheng, S. H. Yang and C. S. Hsu, *Chem. Rev.*, 2009, **109**, 5868–5923.
9 A. Facchetti, *Mater. Today*, 2013, **16**, 123–132.
10 L. Wang, D. Fine, D. Sharma, L. Torsi and A. Dodabalapur, *Anal. Bioanal. Chem.*, 2006, **384**, 310–321.
11 P. Lin and F. Yan, *Adv. Mater.*, 2012, **24**, 34–51.
12 O. Knopfmacher, M. L. Hammock, A. L. Appleton, G. Schwartz, J. Mei, T. Lei, J. Pei and Z. Bao, *Nat. Commun.*, 2014, **5**, 2954.
13 X. Liu, Y. Guo, Y. Ma, H. Chen, Z. Mao, H. Wang, G. Yu and Y. Liu, *Adv. Mater.*, 2014, **26**, 3631–3636.
14 S. Allard, M. Forster, B. Souharce, H. Thiem and U. Scherf, *Angew. Chem., Int. Ed.*, 2008, **47**, 4070–4098.
15 W. L. Leong, N. Mathews, B. Tan, S. Vaidyanathan, F. Dotz and S. Mhaisalkar, *J. Mater. Chem.*, 2011, **21**, 5203–5214.
16 I. Osaka, G. Sauve, R. Zhang, T. Kowalewski and R. D. McCullough, *Adv. Mater.*, 2007, **19**, 4160–4165.
17 Y. Li, S. P. Singh and P. Sonar, *Adv. Mater.*, 2010, **22**, 4862–4866.
18 Y. Li, P. Sonar, S. P. Singh, M. S. Soh, M. M. Van and J. Tan, *Polym. Prepr.*, 2011, **52**, 941–942.
19 Y. Li, P. Sonar, S. P. Singh, M. S. Soh, M. M. Van and J. Tan, *J. Am. Chem. Soc.*, 2011, **133**, 2198–2204.
20 Y. Li, P. Sonar, S. P. Singh, W. Zeng and M. S. Soh, *J. Mater. Chem.*, 2011, **21**, 10829–10835.
21 P. Sonar, S. P. Singh, Y. Li, Z. Ooi, T. Ha, I. Wong, M. S. Soh and A. Dodabalapur, *Energy Environ. Sci.*, 2011, **4**, 2288–2296.
22 I. Meager, R. S. Ashraf, S. Rossbauer, H. Bronstein, J. E. Donaghey, J. Marshall, B. C. Schroeder, M. Heeney, T. D. Anthopoulos and I. McCulloch, *Macromolecules*, 2013, 5961–5967.
23 A. Tang, L. Li, Z. Lu, J. Huang, H. Jia, C. Zhan, Z. Tan, Y. Li and J. Yao, *J. Mater. Chem. A*, 2013, **1**, 5747–5757.
24 M. Se'vignon, J. Papillon, E. Schulz and M. Lemaire, *Tetrahedron Lett.*, 1999, **40**, 5873–5876.
25 Q. Wang, R. Takita, Y. Kikuzaki and F. Ozawa, *J. Am. Chem. Soc.*, 2010, **132**, 11420–11421.
26 L. G. Mercier and M. Leclerc, *Acc. Chem. Res.*, 2013, **46**, 1597–1605.
27 M. P. Ouattara, S. Lenfant, D. Vuillaume, M. Pézolet, J.-F. Rioux-Dubé, J. Brisson and M. Leclerc, *Macromolecules*, 2013, **46**, 6408–6418.
28 D. J. Burke and D. J. Lipomi, *Energy Environ. Sci.*, 2013, **6**, 2053–2066.
29 D. H. Wang, A. Pron, M. Leclerc and A. J. Heeger, *Adv. Funct. Mater.*, 2013, **23**, 1297–1304.
30 M. Kuramochi, J. Kuwabara, W. Lu and T. Kanbara, *Macromolecules*, 2014, **47**, 7378–7385.
31 J.-R. Pouliot, B. Sun, M. Leduc, A. Najari, Y. Li and M. Leclerc, *Polym. Chem.*, 2015, **6**, 278–282.
32 A. Luzio, D. Fazzi, F. Nübling, R. Matsidik, A. Straub, H. Komber, E. Giussani, S. E. Watkins, M. Barbatti, W. Thiel, E. Gann, L. Thomsen, C. R. McNeill, M. Caironi and M. Sommer, *Chem. Mater.*, 2014, **26**, 6233–6240.
33 R. Matsidik, H. Komber, A. Luzio, M. Caironi and M. Sommer, *J. Am. Chem. Soc.*, 2015, **137**, 6705–6711.
34 N. Blouin, A. Michaud, D. Gendron, S. Wakim, E. Blair, R. Neagu-Plesu, M. Belletête, G. Durocher, Y. Tao and M. Leclerc, *J. Am. Chem. Soc.*, 2008, **130**, 732–742.
35 I. Osaka, R. Zhang, G. Sauve, D.-M. Smilgies, T. Kowalewski and R. D. McCullough, *J. Am. Chem. Soc.*, 2009, **131**, 2521–2529.
36 X. Guo, J. Quinn, Z. Chen, H. Usta, Y. Zheng, Y. Xia, J. W. Hennek, R. P. Ortiz, T. J. Marks and A. Facchetti, *J. Am. Chem. Soc.*, 2013, **135**, 1986–1996.
37 S. Chen, B. Sun, W. Hong, H. Aziz, Y. Meng and Y. Li, *J. Mater. Chem. C*, 2014, **2**, 2183–2190.
38 W. Hong, S. Chen, B. Sun, M. A. Arnould, Y. Meng and Y. Li, *Chem. Sci.*, 2015, **6**, 3225–3235.
39 B. Fu, C.-Y. Wang, B. D. Rose, Y. Jiang, M. Chang, P.-H. Chu, Z. Yuan, C. Fuentes-Hernandez, B. Kippelen, J.-L. Brédas, D. M. Collard and E. Reichmanis, *Chem. Mater.*, 2015, **27**, 2928–2937.
40 A. E. Rudenko, C. A. Wiley, S. M. Stone, J. F. Tannaci and B. C. Thompson, *J. Polym. Sci. Part A: Polym. Chem.*, 2012, **50**, 3691–3697.
41 Q. Guo, J. Dong, D. Wan, D. Wu and J. You, *Macromol. Rapid Commun.*, 2013, **34**, 522–527.
42 A. E. Rudenko, C. a. Wiley, J. F. Tannaci and B. C. Thompson, *J. Polym. Sci. Part A: Polym. Chem.*, 2013, **51**, 2660–2668.
43 F. Lombeck, H. Komber, S. I. Gorelsky and M. Sommer, *ACS Macro Lett.*, 2014, **3**, 819–823.
44 S. Pivsa-Art, T. Satoh, Y. Kawamura, M. Miura and M. Nomura, *Bull. Chem. Soc. Jpn.*, 1998, **71**, 467–473.
45 A. Mori, A. Sekiguchi, K. Masui, T. Shimada, M. Horie, K. Osakada, M. Kawamoto and T. Ikeda, *J. Am. Chem. Soc.*, 2003, **125**, 1700–1701.
46 F. Derridj, A. L. Gottumukkala, S. Djebbar and H. Doucet, *Eur. J. Inorg. Chem.*, 2008, 2550–2559.
47 J. Roger, F. Požgan and H. Doucet, *J. Org. Chem.*, 2009, **74**, 1179–1186.
48 F. Shibahara, E. Yamaguchi and T. Murai, *J. Org. Chem.*, 2011, **76**, 2680–2693.
49 X. W. Liu, J. L. Shi, J. X. Yan, J. B. Wei, K. Peng, L. Dai, C. G. Li, B. Q. Wang and Z. J. Shi, *Org. Lett.*, 2013, **15**, 5774–5777.
50 L. Chen, C. Bruneau, P. H. Dixneuf and H. Doucet, *ChemCatChem*, 2013, **5**, 1956–1963.

51 S. Tani, T. N. Uehara, J. Yamaguchi and K. Itami, *Chem. Sci.*, 2014, **5**, 123.
52 P. Chávez, C. Ngov, P. de Frémont, P. Lévêque and N. Leclerc, *J. Org. Chem.*, 2014, **79**, 10179–10188.
53 E. Ö. Karaca, N. Gürbüz, İ. Özdemir, H. Doucet, O. Şahin, O. Büyükgüngör and B. Çetinkaya, *Organometallics*, 2015, **34**, 2487–2493.
54 W. Lu, J. Kuwabara and T. Kanbara, *Polym. Chem.*, 2012, **3**, 3217.
55 Q. Wang, M. Wakioka and F. Ozawa, *Macromol. Rapid Commun.*, 2012, **33**, 1203–1207.
56 Y. Fujinami, J. Kuwabara, W. Lu, H. Hayashi and T. Kanbara, *ACS Macro Lett.*, 2012, **1**, 67–70.
57 W. Lu, J. Kuwabara and T. Kanbara, *Macromolecules*, 2011, **44**, 1252–1255.
58 Y. Fujinami, J. Kuwabara, W. Lu, H. Hayashi and T. Kanbara, *ACS Macro Lett.*, 2012, **1**, 67–70.
59 A. E. Rudenko and B. C. Thompson, *J. Polym. Sci. Part A: Polym. Chem.*, 2015, **53**, 135–147.
60 F. Lombeck, H. Komber, S. I. Gorelsky and M. Sommer, *ACS Macro Lett.*, 2014, **3**, 819–823.
61 P.-O. Morin, T. Bura, B. Sun, S. I. Gorelsky, Y. Li and M. Leclerc, *ACS Macro Lett.*, 2015, **4**, 21–24.
62 J. R. Matthews, W. Niu, A. Tandia, A. L. Wallace, J. Hu, W.-Y. Lee, G. Giri, S. C. B. Mannsfeld, Y. Xie, S. Cai, H. H. Fong, Z. Bao and M. He, *Chem. Mater.*, 2013, **25**, 782–789.
63 Y. He, C. Guo, B. Sun, J. Quinn and Y. Li, *Polym. Chem.*, 2015, **6**, 6689–6697.
64 H. Sirringhaus, P. J. Brown, R. H. Friend, M. M. Nielsen, K. Bechgaard, B. M. W. Langeveld-Voss, A. J. H. Spiering, R. A. J. Janssen, E. W. Meijer, P. Herwig and D. M. de Leeuw, *Nature*, 1999, **401**, 685–688.
65 B. S. Ong, Y. Wu, Y. Li, P. Liu and H. Pan, *Chem. – Eur. J.*, 2008, **14**, 4766–4778.
66 B. W. D'Andrade, S. Datta, S. R. Forrest, P. Djurovich, E. Polikarpov and M. E. Thompson, *Org. Electron.*, 2005, **6**, 11–20.
67 H. Usta, W. C. Sheets, M. Denti, G. Generali, R. Capelli, S. Lu, X. Yu, M. Muccini and A. Facchetti, *Chem. Mater.*, 2014, **26**, 6542–6556.